

Design and Development of a Burst Acquisition System for Geosynchronous Satcom Channels – Final Report (2009-2010)

Project Investigator: K. Vasudevan

Associate Professor

email: vasu@iitk.ac.in



Department of Electrical Engineering

Indian Institute of Technology

Kanpur - 208 016

INDIA

October 2015

Design and Development of a Burst Acquisition System for Geosynchronous Satcom Channels – Final Report (2009-2010)

Project Investigator: K. Vasudevan

Abstract

The key contribution of this work is to develop transmitter and receiver algorithms in discrete-time for turbo-coded offset QPSK signals. The proposed synchronization and detection techniques perform effectively at an SNR per bit close to 1.5 dB, in the presence of a frequency offset as large as 30 % of the symbol-rate and a clock offset of 25 ppm (parts per million). Due to the use of up-sampling and matched filtering and a feedforward approach, the acquisition time for clock recovery is just equal to the length of the preamble. The carrier recovery algorithm does not exhibit any phase ambiguity, alleviating the need for differentially encoding the data at the transmitter. The proposed techniques are well suited for discrete-time implementation.

Index Terms

Offset QPSK (quadrature phase shift keying), frequency offset, clock offset, synchronization, matched filtering, additive white Gaussian noise (AWGN).

I. INTRODUCTION

Geosynchronous satellites provide line-of-sight communications with the ground stations. Such communication links offer distortionless transmission, with the only impairment being AWGN. Whereas transmit power is not so much of an issue at the ground station, it is a precious commodity on-board the satellite. With the growing demand for satellite broadcast services, it has become necessary for the end users to receive signals directly from the satellite. This calls for a vastly reduced size and cost of the receiving equipment at the ground station (which is usually the users premises or the handset) and superior modulation, coding and synchronization techniques. With the discovery of turbo codes, the aforementioned scenario has become a reality.

In order to further improve the performance and bring down the cost of the receivers, we propose offset QPSK as the modulation technique, which allows the use of power efficient non-linear amplifiers and data-aided synchronization algorithms which have a faster acquisition time than the non-data-aided counterparts proposed in [1]. We also use the upsampled version of the matched filter as an interpolator [2], enabling the implementation of a feedforward timing acquisition method, that is faster than the feedback approach discussed

This project is supported by Defence Electronics Applications Lab (DEAL), Dehradun (ref. no. DEAL/02/4043/2005-2006/02/016). The project investigator is with the Dept. of Electrical Engg., Indian Institute of Technology, Kanpur. Email: vasu@iitk.ac.in

in [1]. Though there are other interpolation techniques [3], [4] for timing acquisition, we believe that they are well suited for feedback methods.

Before we proceed, a brief review of the literature on carrier and timing synchronization is in order. An improved phase lock loop that operates effectively at medium to low SNR is proposed in [5]. A data-aided carrier recovery loop for duobinary encoded offset QPSK is given in [6]. A tutorial on carrier and timing synchronization is given in [7]. Joint carrier recovery and equalization of digitally modulated signals is discussed in [8], [9]. A data-aided carrier recovery algorithm for estimating phase and frequency offsets is discussed in [10], [11] and also in [12], [13] for digital land mobile radio and satellite communication. Detection of bursty QPSK signals at low SNR is described in [14]. A digital modem for offset-QPSK is dealt with in [15]. Carrier synchronization for trellis-coded signals is given in [16]. A digital PLL for QPSK signals is described in [17] and an all-digital implementation of carrier synchronization for digital radio systems is proposed in [18]. A comparison of different carrier recovery techniques is presented in [19]. A carrier recovery algorithm for M -ary QAM with a capability to track large frequency offsets is discussed in [20]. A non-data-aided carrier recovery method for modified 128-QAM is proposed in [21].

Timing recovery can be broadly classified into synchronous and asynchronous methods. In the synchronous methods, the local clock at the receiver is regenerated from the incoming signal. Such techniques are implemented in hardware and are usually employed in analog modems [22]. In the asynchronous approach, the local clock at the receiver is free running, due to which the ratio of the receiver sampling frequency to the incoming symbol-rate is not an integer. If this ratio were to be an integer (equal to say, M), then timing acquisition alone would have sufficed – we could recover the symbols from the matched filter output every M^{th} sample. Let us denote the sampling epoch as m_0 modulo- M . However, in practical situations the transmitter and receiver clocks are asynchronous (their frequencies are not exactly identical), therefore the above mentioned ratio is not an integer. Hence timing needs to be acquired and tracked (this is explained in the next para and in section III-C). In the present context, the word “timing” implies knowing when to recover the symbols from the matched filter output. In the asynchronous methods of timing recovery, signal processing techniques are used which are suitable for software implementation [23]–[25].

The transmit and receive clocks are usually specified as F_0 Hz, $\pm\delta$ parts per million (ppm). This implies that the actual frequency of the transmit and receive clocks lies in the range $F_0(1 \pm \delta \times 10^{-6})$ Hz. The worst case frequency difference is $\pm 2F_0\delta \times 10^{-6}$ Hz. For ease of understanding, we could assume that the transmit clock is exact (F_0 Hz) and the receive clock is F_0 Hz, $\pm 2\delta$ ppm. Let us now assume that the transmitted signal is sampled using the exact clock (with frequency F_0 Hz) and 10^6 samples are obtained over a period of time. If the same transmitted signal is sampled using the receive clock (having an accuracy of $\pm 2\delta$ ppm) over the same time interval, we would obtain $10^6 \pm 2\delta$ samples. For example, if $\delta = 0.5$, then we would obtain one sample more or less over 10^6 samples, which further implies that the sampling epoch would change by one sample over 10^6 samples (the new sampling epoch would be $(m_0 \pm 1)$ modulo- M).

More recently, iterative timing recovery is proposed in [26]. The Cramér-Rao bound for non-data-aided timing recovery for linearly modulated signals with no ISI is presented in [27].

This paper is organized as follows. Section II discusses the system model. In Section III we discuss the receiver algorithms. The performance results are discussed in Section IV. Finally, in Section V we present our

conclusions.

II. SYSTEM MODEL

Preamble	Data	Postamble
L_p	L_d	L_o

Fig. 1. The burst structure.

We assume that the data to be transmitted is organized into bursts (or frames). The burst consists of a known preamble of length L_p (QPSK) symbols, followed by turbo-coded data of length L_d symbols and a known postamble of length L_o symbols. Thus, the total length of the frame is

$$L = L_p + L_d + L_o. \quad (1)$$

The L_d QPSK symbols are obtained by passing an uncoded bit stream through a rate-1/2 turbo code. The generator matrix of each of the constituent encoders is given by [28]:

$$\mathbf{G}(D) = \begin{bmatrix} 1 & \frac{1+D^2+D^3+D^4}{1+D+D^4} \end{bmatrix}. \quad (2)$$

The received signal can be written as:

$$r(t) = \sqrt{4/T} \Re \left\{ \tilde{s}(t) e^{j[2\pi(F_c + \Delta F)t + \theta_0]} \right\} + w_1(t) \quad (3)$$

where $\Re\{\cdot\}$ denotes the real-part, $1/T$ is the baud-rate, F_c is the nominal carrier frequency, ΔF is the frequency offset (which can be positive or negative), θ_0 is the carrier phase and $w_1(t)$ is additive white Gaussian noise with two-sided power spectral density $N_0/2$ (watts/Hz). The term $\tilde{s}(t)$ (we use tilde to denote complex quantities) in (3) is the complex envelope of the offset QPSK signal and is given by:

$$\begin{aligned} \tilde{s}(t) &= s_I(t) + j s_Q(t) \\ &= \sum_{k=0}^{L-1} S_{k,I} p(t - kT - \alpha) \\ &\quad + j \sum_{k=0}^{L-1} S_{k,Q} p(t - kT - T/2 - \alpha) \end{aligned} \quad (4)$$

where $S_{k,I} \in \pm 1$ and $S_{k,Q} \in \pm 1$ are the in-phase and quadrature components of the QPSK symbol and $p(t)$ is the impulse response of the transmit filter, which is assumed to have the root-raised cosine spectrum with 40% roll-off. The variable α denotes the random timing phase which is assumed to be uniformly distributed in $[0, T)$. Observe that $p(t)$ extends over $-\infty < t < \infty$. However in practice, it can be delayed and truncated to obtain a causal and finite impulse response, with negligible intersymbol-interference (ISI) at the matched filter output. The task of the receiver is to estimate the QPSK symbols such that the error-rate is close to the theoretical limit.

Since we deal with discrete-time signals in this paper, the first task is to convert $r(t)$ in (3) into a discrete-time signal. This is accomplished by passing $r(t)$ through a bandpass filter (BPF) followed by bandpass sampling. For convenience of subsequent analysis, we assume an ideal BPF having unit energy with a gain of $\sqrt{T/4}$ in

the passband extending over $[F_c - 1/T, F_c + 1/T]$ Hz. This ensures that the noise power at the BPF output is $N_0/2$. Assuming a sampling frequency of $F_s = 1/T_s$, the bandpass sampling requirements can be stated as follows [29]:

$$\begin{aligned} \frac{2\pi(F_c - 1/T)}{F_s} &\geq k\pi \\ \frac{2\pi(F_c + 1/T)}{F_s} &\leq (k+1)\pi \end{aligned} \quad (5)$$

where k is a positive integer. We assume that the conditions in (5) are satisfied with an equality so that $F_s = 4/T$ or equivalently $T/T_s = 4$. Therefore, the symbols can be delayed by $T/2 \equiv 2$ samples in discrete-time. We further assume that

$$\frac{2\pi F_c}{F_s} = k\pi + \pi/2 = \pi/2 \bmod 2\pi \quad (6)$$

if k is even. Thus the output of the analog-to-digital (A/D) converter after bandpass sampling can be written as

$$r(nT_s) = \Re \left\{ \tilde{s}(nT_s) e^{j[(\pi/2 + \omega_0)n + \theta_0]} \right\} + w(nT_s) \quad (7)$$

where

$$\begin{aligned} \tilde{s}(nT_s) &= \tilde{s}(t)|_{t=nT_s} \\ &= s_I(nT_s) + j s_Q(nT_s) \\ w(nT_s) &= w(t)|_{t=nT_s} \\ \omega_0 &= 2\pi\Delta F/F_s \end{aligned} \quad (8)$$

where $w(t)$ is noise at the BPF output. Note that $w(nT_s)$ denotes samples white Gaussian noise with variance $N_0/2$. The simulation model of the transmitter and its input are illustrated in Figures 2 and 3.

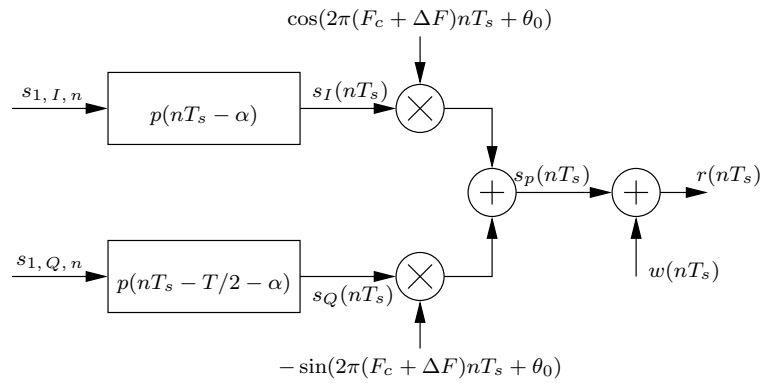


Fig. 2. Simulation model of the transmitter.

Having assumed that $T/T_s = 4$, it is now necessary to find out what is the maximum frequency offset that can be tolerated. With 40% roll-off, the bandwidth of the complex baseband signal is $1.4/(2T) = 0.7/T$. The spectrum of the discrete-time sampled signal is shown in Figure 4, when the frequency-offset $\Delta F = 0$. Here

$$\begin{aligned} \omega_1 &= \pi/2 - 2\pi \times 0.7/(TF_s) = 0.15\pi \\ \omega_2 &= \pi/2 + 2\pi \times 0.7/(TF_s) = 0.85\pi = \pi - \omega_1. \end{aligned} \quad (9)$$

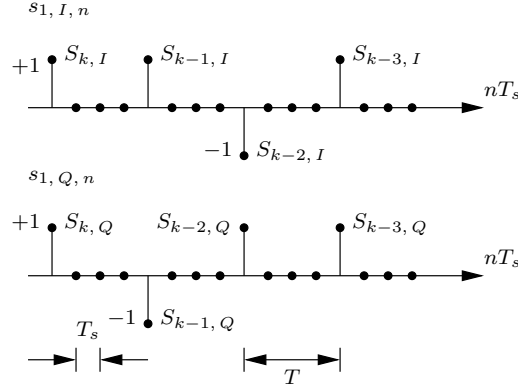


Fig. 3. Symbol sequence input to the transmitter. Here $T/T_s = M = 4$.

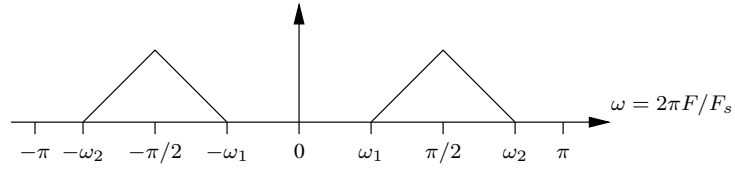


Fig. 4. The spectrum of the discrete-time sampled signal with $\Delta F = 0$.

In order to avoid aliasing of the spectrum, we require

$$\begin{aligned} |2\pi\Delta F/F_s| &\leq \omega_1 \\ \Rightarrow |\omega_0| &\leq \omega_1. \end{aligned} \quad (10)$$

Substituting for ω_1 from (9) and using $T/T_s = 4$, we obtain

$$|\Delta F| \leq 0.3/T \quad (11)$$

which is less than or equal to 30% of the symbol-rate. Having justified the maximum frequency offset used in this work, we next discuss the procedure for simulating the clock offset.

Assume that $r(t)$ in (3) is sampled at a rate of

$$F'_s = F_s(1 \pm 2\delta \times 10^{-6}). \quad (12)$$

The corresponding sampling period is:

$$T'_s = 1/F'_s = T_s(1 \mp 2\delta \times 10^{-6}) \triangleq T_s + \epsilon. \quad (13)$$

Then

$$r(nT'_s) = \Re \left\{ \tilde{s}(nT'_s) e^{j[2\pi(F_c + \Delta F)nT'_s + \theta_0]} \right\} + w_1(nT'_s). \quad (14)$$

Define

$$\omega_3 = 2\pi \frac{\Delta F \mp (F_c + \Delta F)2\delta \times 10^{-6}}{F_s}. \quad (15)$$

Then

$$r(nT'_s) = \Re \left\{ \tilde{s}(nT'_s) e^{j[(\pi/2 + \omega_3)n + \theta_0]} \right\} + w_1(nT'_s). \quad (16)$$

Thus, one of the effects of having an error in the sampling frequency is to introduce an additional frequency offset equal to:

$$\mp 2\pi \frac{(F_c + \Delta F)2\delta \times 10^{-6}}{F_s} \quad \text{radians.} \quad (17)$$

Henceforth, we assume that $|\omega_3| \leq \omega_1$ to avoid aliasing (see also (10)). We now study the effect of T'_s on the complex baseband signal $\tilde{s}(\cdot)$ in (16).

We have

$$\begin{aligned} \tilde{s}(nT'_s) &= \sum_{k=0}^{L-1} S_{k,I} p(nT'_s - kT - \alpha) \\ &\quad + j \sum_{k=0}^{L-1} S_{k,Q} p(nT'_s - kT - T/2 - \alpha) \end{aligned} \quad (18)$$

Let the impulse response of the transmit filter extend over $[0, N]$ samples, at a sampling rate of $F_s = 4/T$. Let

$$nT_s - kT = iT_s \quad (19)$$

where i is an integer. Using (13), (18) can be rewritten as:

$$\begin{aligned} \tilde{s}(nT'_s) &= \sum_{k=0}^{L-1} S_{k,I} p(nT_s + n\epsilon - kT - \alpha) \\ &\quad + j \sum_{k=0}^{L-1} S_{k,Q} p(nT_s + n\epsilon - kT - T/2 - \alpha) \\ &= \sum_{i=0}^N p(iT_s + n\epsilon - \alpha) S_{(n-i)/4, I} \\ &\quad + j \sum_{i=0}^N p(iT_s + n\epsilon - T/2 - \alpha) S_{(n-i)/4, Q} \end{aligned} \quad (20)$$

where it is understood that $S_{(n-i)/4, I}$ and $S_{(n-i)/4, Q}$ are non-zero every 4^{th} value of n , all other values are zero (see Figure 3).

The above equation suggests that the complex baseband signal must be generated using time-varying transmit filter coefficients [30]. Note that if $\epsilon = 0$, the transmit filter would be time-invariant, since α is a constant for a given burst. Clearly, it doesn't make sense to allow $n\epsilon$ to grow without bound. In fact, it needs to be periodically "normalized". How this is done, is shown in Figure 5, for generating the in-phase part of the complex baseband [30]. The sequence $s_{1,I,n}$ is illustrated in Figure 3. The procedure for generating the quadrature part of the complex baseband is similar. Note that the signal $s_I(nT'_s)$ obtained from Figure 5(b) is approximately equal to that obtained in parts (c) and (d), as long as the first and the last transmit filter coefficients contribute insignificantly to the energy of the overall transmit filter. This can be ensured by having a large enough N . The simulation model for the transmitter is similar to Figure 2 with T_s replaced by T'_s . Since $T'_s \approx T_s$, we continue to assume that the samples of $w(nT'_s)$ are uncorrelated with zero mean and variance $N_0/2$. The next step is to discuss the receiver.

III. RECEIVER

Let $\hat{\omega}_3$ and $\hat{\omega}_f$ denote the "coarse" and the "fine" estimates of the frequency offset respectively, corresponding to the sampling frequency of $1/T_s$. The receiver in Figure 6 operates in the following steps:

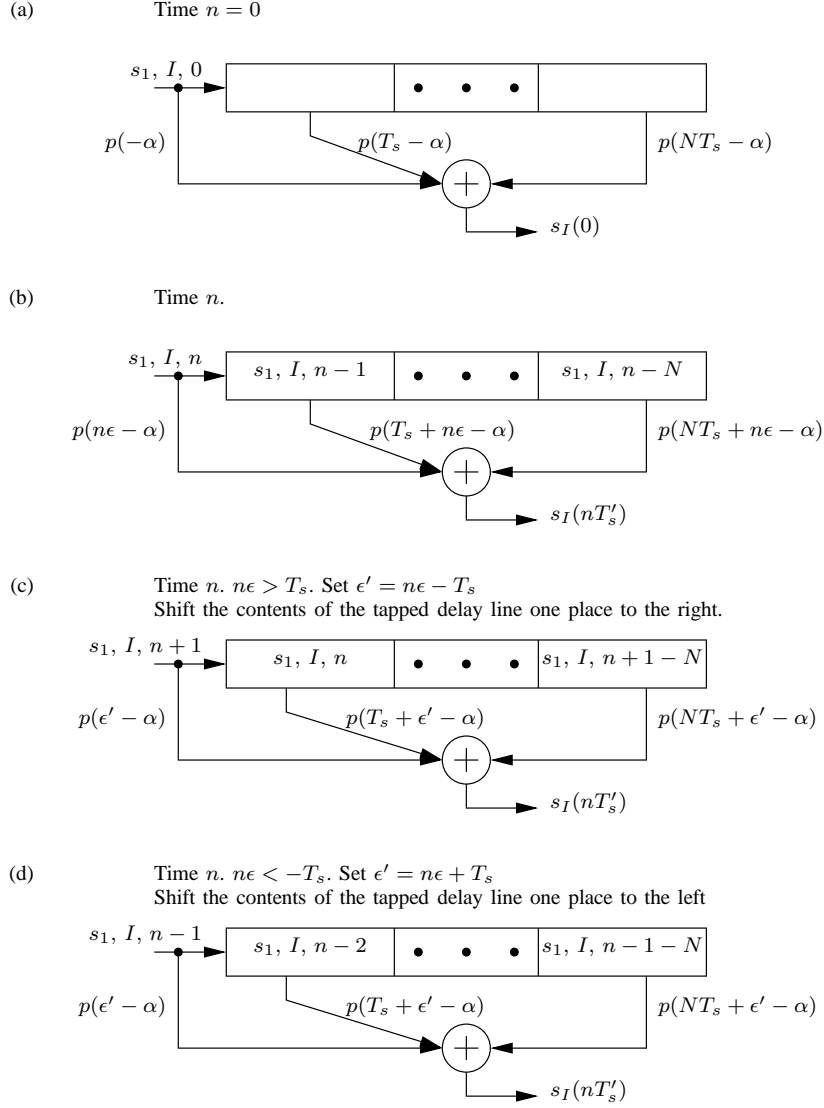


Fig. 5. Illustrating the process of generating $s_I(nT'_s)$ (a) Time $n = 0$. (b) Time n . (c) Adjustments at time n when $n\epsilon > T_s$. (d) Adjustments at time n when $n\epsilon < -T_s$.

- 1) Demodulate $r(nT'_s)$ with $\hat{\omega}_3 = \hat{\omega}_f = 0$ in Figure 6 and detect the start of frame using the “differential” correlation method. Store the samples $r(nT'_s)$ corresponding to a frame. Index the first incoming sample as 0, the next sample as 1 and so on. Obtain a coarse estimate of the frequency offset and denote it as $\hat{\omega}_3$.
- 2) Demodulate the stored values of $r(nT'_s)$ using $\pi/2 + \hat{\omega}_3$. Estimate the start of frame for the second time using the differential correlation method.
- 3) Obtain the maximum likelihood estimate of the residual frequency offset which is equal to $\omega_f = \omega_3 - \hat{\omega}_3$. Denote this estimate as $\hat{\omega}_f$.
- 4) Demodulate the stored values of $r(nT'_s)$ using $\pi/2 + \hat{\omega}_3 + \hat{\omega}_f$. Estimate the start of frame for the third time using the correlation method. Estimate the symbol amplitude, θ_0 and the variance of additive noise.
- 5) Detect the data using the turbo decoder. Track the timing and carrier phase resulting due to the clock

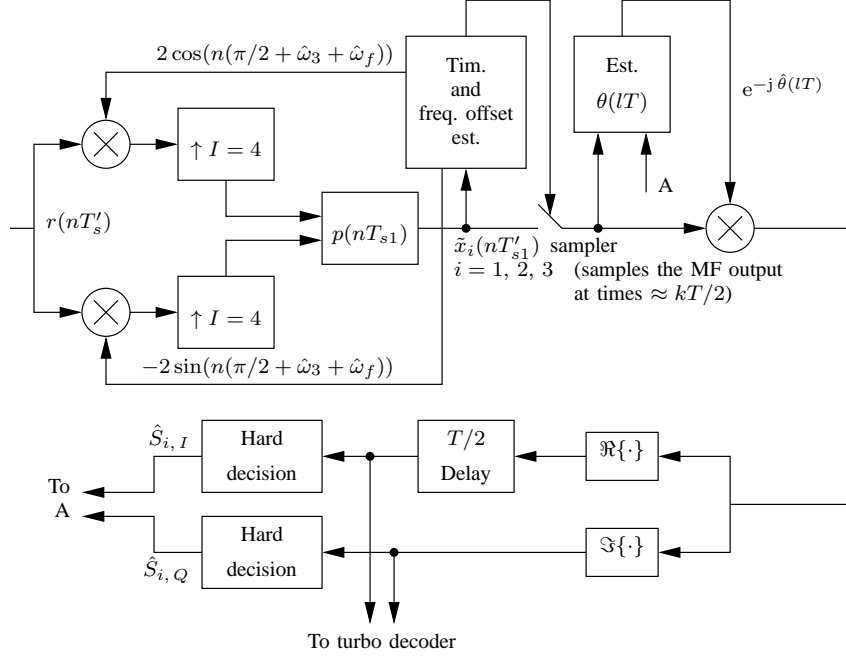


Fig. 6. The discrete-time receiver which up-samples the local oscillator output by a factor of I and then performs matched filtering at a sampling frequency F_{s1} .

offset and residual frequency offset given by $\omega_f - \hat{\omega}_f$ respectively.

Before we proceed to elaborate on the above steps, let us look into the operation of up-sampling and matched filtering [31].

A. Up-Sampling and Matched Filtering

For ease of exposition, we assume that $\delta = 0$ ($T'_s = T_s$). The samples of the transmitted pulse is shown in Figure 7(a) by solid impulses (Kronecker delta function). We assume that $p(t - \alpha)$ spans over $N + 1 (= 13)$ ($0 \leq n \leq N$) samples and the sampling frequency $1/T_s$ is such that it satisfies the Nyquist criterion for no aliasing of the spectrum of $p(t)$. The corresponding discrete-time matched filter is shown in Figure 7(b) by solid impulses. The matched filter output can be obtained using the frequency-domain approach. Let $P(F)$ denote the Fourier transform of $p(t)$, assumed to be bandlimited to $|F| \leq B$. Then the discrete-time Fourier transform of $p(nT_s - \alpha)$ is obtained as follows:

$$\begin{aligned}
 p(t - \alpha) &= g(t) \\
 &\Rightarrow \tilde{G}(F) \\
 &= \begin{cases} \tilde{P}(F)e^{-j2\pi F\alpha} & -B \leq F \leq B \\ 0 & \text{otherwise} \end{cases}
 \end{aligned} \tag{21}$$

Therefore

$$\begin{aligned}
 p(nT_s - \alpha) &= g(nT_s) \\
 &\Rightarrow \tilde{G}_{\mathcal{P}}(F)
 \end{aligned}$$

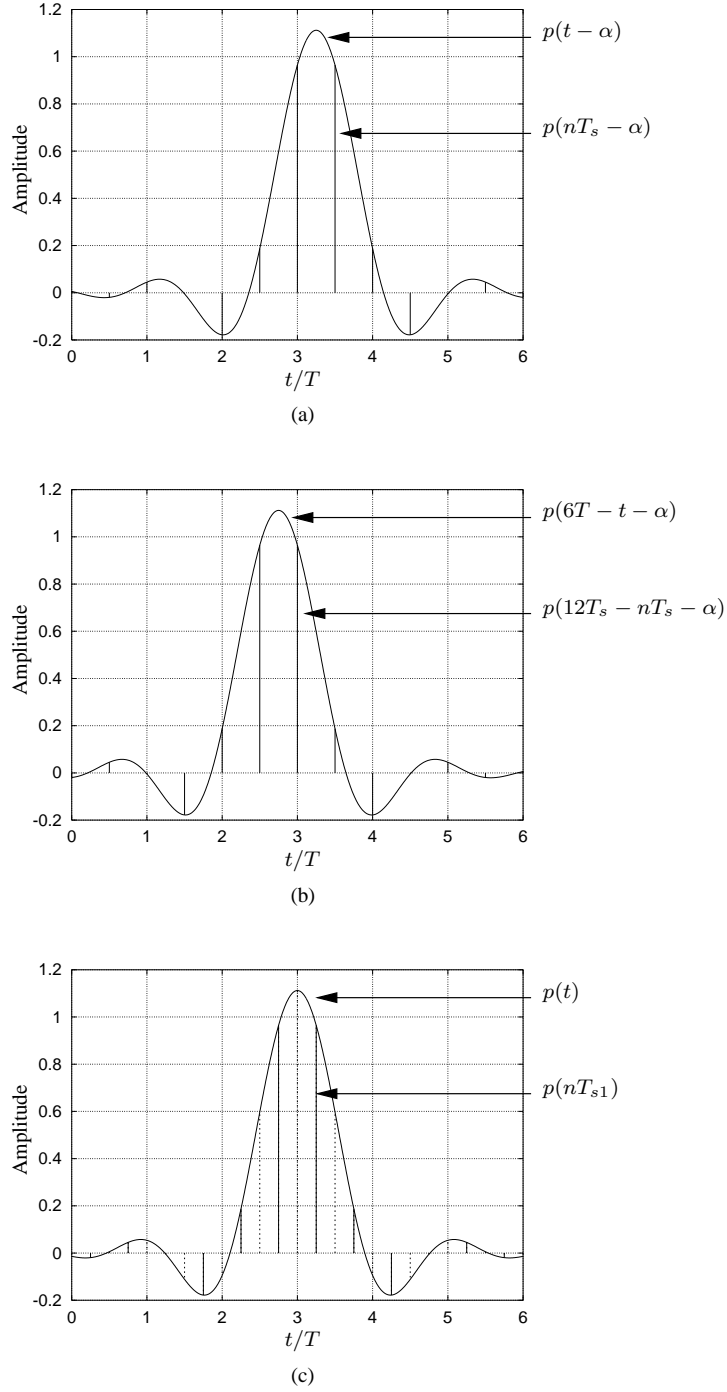


Fig. 7. (a) The received pulse $p(t - \alpha)$ and its samples taken at $T/T_s = 2$. $\alpha = T_s/4$. (b) Filter matched to the received pulse $p(6T - t - \alpha)$ and its samples taken at $T/T_s = 2$. (c) Filter matched to $p(t)$ (in this case is $p(6T - t) = p(t)$ itself) sampled at a higher frequency $T/T_{s1} = 4$. Observe that one set of samples (shown by solid impulses) correspond to the samples of the matched filter in part (b), for $\alpha = T_s/4$.

$$= \begin{cases} \tilde{G}(F)/T_s & 0 \leq |F| \leq B \\ 0 & B \leq |F| \leq F_s/2 \end{cases} \quad (22)$$

where $\tilde{G}_{\mathcal{P}}(F)$ denotes a periodic function of frequency, that is [29]

$$\tilde{G}_{\mathcal{P}}(F) = \tilde{G}_{\mathcal{P}}(F + kF_s) = \frac{1}{T_s} \sum_{i=-\infty}^{\infty} \tilde{G}(F - iF_s). \quad (23)$$

Now, when $p(nT_s - \alpha)$ is convolved with $p(NT_s - \alpha - nT_s)$, the peak occurs at $t = NT_s$, independent of α . Note that $p(NT_s - \alpha - nT_s)$ represents the discrete-time causal matched filter for $p(nT_s - \alpha)$. The peak value is equal to $R_{pp}(0)/T_s$ [29], where $R_{pp}(t)$ is the continuous-time autocorrelation of $p(t)$. In practice however since the receiver does not know α , it is not possible to obtain the exact matched filter as in Figure 7(b). The solution lies in sampling $p(NT_s - t)$ at a higher frequency (say $F_{s1} = 1/T_{s1}$) compared to $1/T_s$, as illustrated in Figure 7(c).

Let us denote $T_s/T_{s1} = I$ which is referred to as the interpolation factor. Construct the up-sampled sequence from the incoming signal $p(nT_s - \alpha)$ as follows:

$$g_1(nT_{s1}) = \begin{cases} g(nT_s/I) & \text{for } n = mI \\ 0 & \text{otherwise} \end{cases} \quad (24)$$

where $g(nT_s)$ is defined in (22). The discrete-time Fourier transform (DTFT) of $g_1(nT_{s1})$ is [32]:

$$g_1(nT_{s1}) \Rightarrow G_{\mathcal{P}}(FI). \quad (25)$$

Let us define a new frequency variable $F_1 = FI$ with respect to the new sampling frequency F_{s1} . Now, if $p(NT_s - t)$ is sampled at a rate F_{s1} the DTFT of the resulting sequence is:

$$p(NT_s - nT_{s1}) = g_2(nT_{s1}) \Rightarrow \tilde{G}_{\mathcal{P},2}(F_1) \quad (26)$$

where

$$\begin{aligned} & \tilde{G}_{\mathcal{P},2}(F_1) \\ &= \begin{cases} \frac{\tilde{P}^*(F_1)}{T_{s1}} e^{-j2\pi F_1 NT_s} & 0 \leq |F_1| \leq B \\ 0 & B \leq |F_1| \leq F_{s1}/2. \end{cases} \end{aligned} \quad (27)$$

The convolution of $g_1(nT_{s1})$ with $g_2(nT_{s1})$ can be written as [29]:

$$\begin{aligned} & g_1(nT_{s1}) \star g_2(nT_{s1}) \\ &= \frac{1}{T_s T_{s1} F_{s1}} \int_{F_1=-B}^B \left| \tilde{P}(F_1) \right|^2 \\ & \quad \times e^{j2\pi F_1 (nT_{s1} - \alpha - NIT_{s1})} dF_1. \end{aligned} \quad (28)$$

Clearly if $\alpha = n_0 T_{s1}$, where n_0 is an integer, the above convolution becomes

$$g_1(nT_{s1}) \star g_2(nT_{s1}) = \frac{R_{pp}((n - n_0 - NI)T_{s1})}{T_s} \quad (29)$$

with a peak value equal to $R_{pp}(0)/T_s$, occurring at $(n_0 + NI)T_{s1}$. When α is not an integer multiple of T_{s1} , $R_{pp}(0)$ occurs in between two consecutive samples and we can get close to the peak by increasing I . Henceforth, we assume that the first symbol in the frame occurs at time $\alpha + NIT_{s1}$ and $R_{pp}(0)/T_s = 1$. If

the clock offset $\delta = 0$ then the subsequent symbols can be extracted from the matched filter output at times $(n_0 + NI)T_{s1} + kT/2 = (n_0 + NI)T_{s1} + 2kIT_{s1}$ where we have used the fact that

$$\frac{T}{T_{s1}} = \frac{T}{T_s} \cdot \frac{T_s}{T_{s1}} = 4I. \quad (30)$$

If $\delta \neq 0$, then the sampling instants at the MF output varies with time and needs to be tracked. This aspect will be taken up in subsection III-C. However, the matched filter coefficients are obtained at F_{s1} and not at F'_{s1} , since in practice F'_{s1} is not known at the receiver.

The derivation of the signal at the input and the output of the matched filter in the presence of a frequency offset and clock offset is too involved. We are only interested in the signal at the output of the sampler. This will be taken up in the next subsection.

B. Timing and Carrier Acquisition using the Preamble

This section is an elaboration of the first four steps listed in section III. Recall that in the first step, the start of frame and a coarse estimate of the frequency offset is obtained. The demodulation is done using a local oscillator frequency of $\pi/2$ radians. Let

$$t_0 = \alpha + NIT_{s1} \approx \alpha + NIT'_{s1}. \quad (31)$$

We proceed by making a key observation that at the right instants, the T -spaced sampler output can be approximated as (since $R_{pp}(0)/T_s = 1$):

$$\tilde{x}_1(t_0 + kT) \approx \tilde{\beta}(kT)e^{j(\omega_3 Mk + \theta_0)} + \tilde{v}_1(t_0 + kT) \quad (32)$$

for $0 \leq k \leq L - 1$ where

$$\tilde{\beta}(kT) = S_{k,I} + j\gamma_{k,Q} \quad (33)$$

where $S_{k,I}$ is defined in (4) and $\gamma_{k,Q}$ denotes the intersymbol interference (ISI) in the quadrature arm. Note that, $\gamma_{k,Q}$ is a function of the past, current and future quadrature symbols as given by (see Figure 8):

$$\gamma_{k,Q} = \sum_{j=0}^{2L_{\text{ISI}}-1} S_{k+L_{\text{ISI}}-1-j,Q} h_j \quad (34)$$

where L_{ISI} denotes the span of $R_{pp}(t)$ (in symbol durations) on the either side of $R_{pp}(0)$ and h_j denotes coefficients of the filter having a raised-cosine frequency response. In the simulations, L_{ISI} was taken to be 3.

The term $\tilde{v}(\cdot)$ in (32) denotes samples of zero-mean Gaussian noise with autocorrelation [29]

$$(1/2)E[\tilde{v}_1(kT)\tilde{v}_1^*(kT - mT)] = N_0\delta_K(mT) \quad (35)$$

where $\delta_K(\cdot)$ is the Kronecker delta function. The approximation in (32) is due to the presence of ISI, besides noise. As ω_3 and δ tend to zero, and when t_0 is an integer multiple of T_{s1} , the ISI approaches zero, and the approximation becomes an equality.

Define

$$\begin{aligned} \tilde{\mu}_1(n, k) &= \tilde{x}_1(nT'_{s1})\tilde{\beta}^*(kT) \\ \tilde{y}_1(nT'_{s1}) &= \sum_{i=0}^{L_p-L_{\text{ISI}}-1} \tilde{\mu}_1^*(n + iMI, i) \\ &\quad \times \tilde{\mu}_1(n + (i+1)MI, i+1). \end{aligned} \quad (36)$$

$$R_i = \frac{|\tilde{y}_1(n_1 T'_{s1})|^2_i}{\langle |\tilde{y}_1(n T'_{s1})|^2 \rangle_i} \quad (40)$$

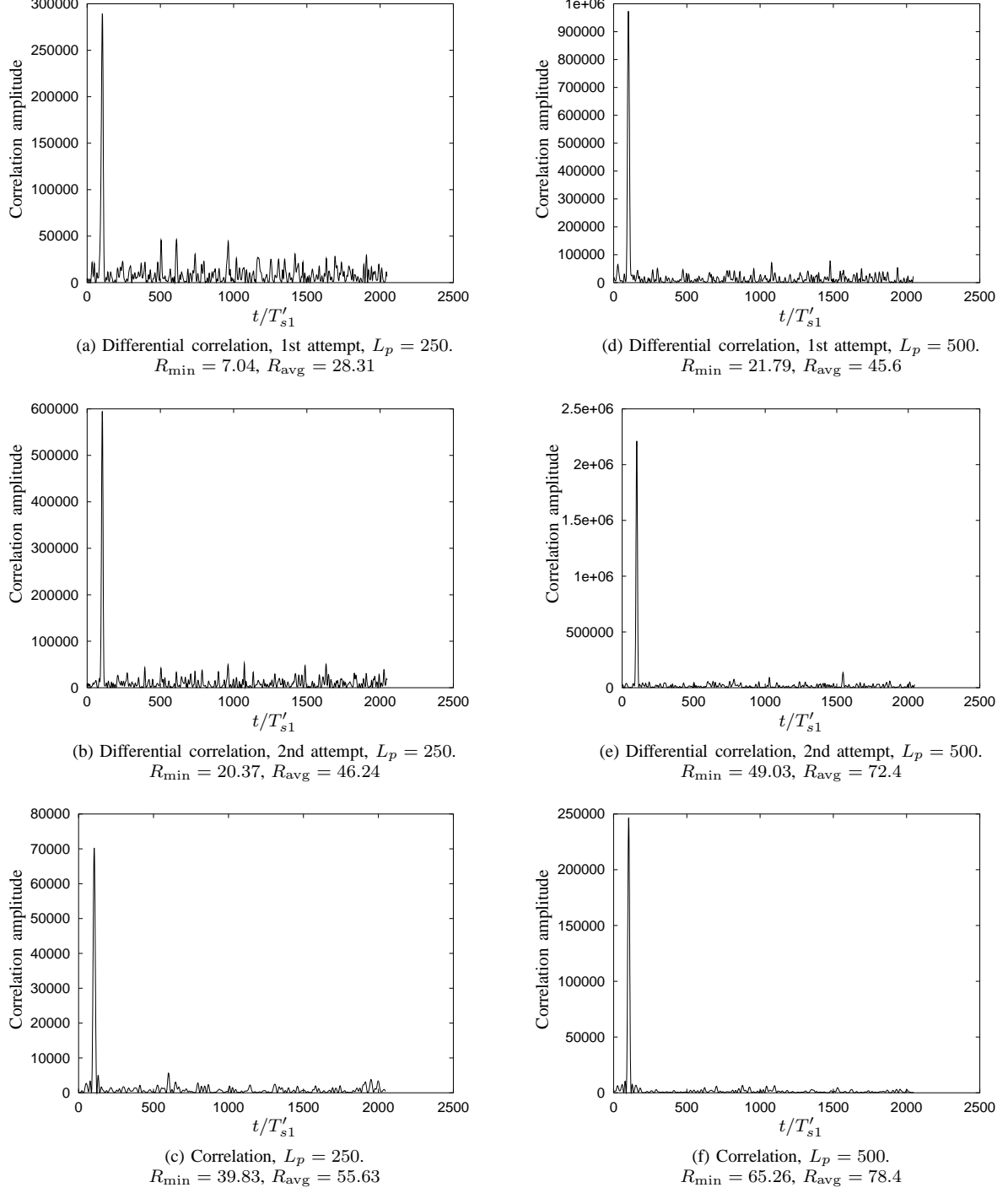


Fig. 9. Frame detection at 1 dB SNR for preamble lengths of $L_p = 250$ and $L_p = 500$.

where $\langle \cdot \rangle$ denotes the time-average. In the simulations, the time average was computed over 2048 samples (spaced at T'_{s1}), which includes the peak value. It is convenient to define R_{avg} and R_{\min} , which are the average and minimum values of R_i over several frames. In Figure 9 R_{\min} and R_{avg} were computed over 10^5 frames. We could also define a threshold slightly less than R_{\min} . A frame could be declared as “detected” if R_i exceeds the threshold.

TABLE I

NORMALIZED VARIANCE OF TIMING ERROR AT AN SNR PER BIT OF 1 DB FOR $L_p = 250$ AND $\alpha = \delta = 0$.

	(a) Differential correlation 1st attempt	(b) Differential correlation 2nd attempt	(c) Correlation
Normalized Variance	9.7×10^{-3}	2.7×10^{-3}	1.5×10^{-3}
Maximum error (samples)	8	3	3

TABLE II

NORMALIZED VARIANCE OF TIMING ERROR AT AN SNR PER BIT OF 1 DB FOR $L_p = 500$ AND $\alpha = \delta = 0$.

	(a) Differential correlation 1st attempt	(b) Differential correlation 2nd attempt	(c) Correlation
Normalized Variance	4.3×10^{-3}	1.3×10^{-3}	6×10^{-4}
Maximum error (samples)	5	2	1

The timing and frequency offset estimates obtained from (37) and (39) are not very accurate when ω_3 is large, e.g. 0.15π radians. This is clear from column (a) in Tables I, III for $L_p = 250$ and II, IV for $L_p = 500$. The main reason is due to the approximation in (32), which gets better as ω_3 gets smaller. This is why we need to estimate the timing and frequency offset for the second time.

The normalized (with respect to T) variance of the timing error in the first attempt of the differential

TABLE III

RMS AND MAXIMUM FREQUENCY OFFSET ESTIMATION ERROR IN RADIANS AT AN SNR PER BIT OF 1 DB FOR $L_p = 250$.

	(a) Differential correlation 1st attempt	(b) Differential correlation 2nd attempt	(c) ML step 1	(d) ML step 2
RMS	0.0286	0.01255	5.91×10^{-4}	1.52×10^{-4}
Max	0.127	0.0565	2.6×10^{-3}	6.75×10^{-4}

TABLE IV

RMS AND MAXIMUM FREQUENCY OFFSET ESTIMATION ERROR IN RADIANS AT AN SNR PER BIT OF 1 DB FOR $L_p = 500$.

	(a) Differential correlation 1st attempt	(b) Differential correlation 2nd attempt	(c) ML step 1	(d) ML step 2
RMS	0.0255	8.8×10^{-3}	5.9×10^{-4}	5.3×10^{-5}
Max	0.087	0.0429	2.8×10^{-3}	2.5×10^{-4}

correlation method is given by

$$\left\langle \left(\frac{n_1 T'_{s1} - t_0}{T} \right)^2 \right\rangle. \quad (41)$$

The average was computed over 10^5 frames. The maximum timing error in samples is given by

$$\max \frac{|n_1 T'_{s1} - t_0|}{T'_{s1}} \quad (42)$$

which is taken over 10^5 frames. Observe that it is necessary to set $\delta = 0$ and α equal to an integer multiple of T'_{s1} (see (29)) to compute (41) and (42). In the simulations, α was set to zero, for computing (41) and (42). The root mean square (rms) error in the frequency offset estimate in the first attempt of the differential correlation method is given by:

$$\sqrt{\langle (\omega_3 - \hat{\omega}_3)^2 \rangle} \quad (43)$$

with the average computed over 10^5 frames. Similarly, the maximum error in the frequency offset estimate for the first attempt is:

$$\max |\omega_3 - \hat{\omega}_3| \quad (44)$$

The second attempt is initiated by first demodulating $r(nT'_s)$ using the local oscillator frequency as $\pi/2 + \hat{\omega}_3$. The resultant frequency offset is $\omega_f = \omega_3 - \hat{\omega}_3$. Let us denote the matched filter output as $\tilde{x}_2(nT'_{s1})$. The effect of applying (37) and (39) again with $\tilde{x}_1(nT'_{s1})$ replaced by $\tilde{x}_2(nT'_{s1})$, is given in column (b) of Tables I, III for $L_p = 250$ and II, IV for $L_p = 500$. While there is a significant improvement in the timing estimate, the accuracy of the frequency offset estimate is still inadequate. For example, in Table IV with $L_p = 500$, the second attempt yields a root mean square (RMS) error equal to 8.8×10^{-3} radians. With $T/T_s = M = 4$, the phase change over 10 symbols is $0.0088 \times 4 \times 10 = 0.352$ radians, which is too fast for a phase tracking loop. This motivates us to use the maximum likelihood (ML) method of estimating ω_f .

Assume that in the second attempt the outcome of (37) with $\tilde{x}_1(nT'_{s1})$ replaced by $\tilde{x}_2(nT'_{s1})$, is $n_2 T'_{s1}$. Observe that $n_2 T'_{s1}$ is the second estimate of t_0 . Then (see also (32))

$$\tilde{x}_2(n_2 T'_{s1} + kT) \approx \tilde{\beta}(kT) e^{j(\omega_f M k + \theta_0)} + \tilde{v}_2(n_2 T'_{s1} + kT). \quad (45)$$

The ML rule for estimating the frequency offset can be stated as follows: set $\hat{\omega}_f = \omega_i$ if ω_i maximizes

$$\left| \sum_{k=0}^{L_p - L_{ISI}} \tilde{x}_2(n_2 T'_{s1} + kT) \tilde{\beta}^*(kT) e^{-j\omega_i M k} \right| \quad (46)$$

where

$$\begin{aligned} \omega_i &= \omega_{\min} + i\omega_s \\ \omega_{\min} &< \omega_i < \omega_{\max} \\ \omega_{\min} &= \hat{\omega}_3 - 0.2 \\ \omega_{\max} &= \hat{\omega}_3 + 0.2 \end{aligned} \quad (47)$$

where $\omega_s = 4 \times 10^{-5}$ radians, denotes the resolution. Observe that the FFT cannot be used in (46), since the search is only over a narrow portion of the digital spectrum in the range $[\hat{\omega}_3 - 0.2, \hat{\omega}_3 + 0.2]$. The reason for

choosing 0.2 radians can be traced to the maximum estimation error in column (a) of Table III, which is equal to 0.127 radians over 10^5 frames. The maximum estimation error over 10^3 frames was found (from simulations) to be 0.091 radians. Thus we find that increase in the number of frames by two orders of magnitude, results in only a marginal increase in the maximum estimation error. Hence we expect the probability of estimation error exceeding 0.2 radians, to be very small. We now discuss the complexity of the ML approach.

For obtaining a resolution of $\omega_s = 4 \times 10^{-5}$ radians, the search interval of 0.4 radians must be divided into 10^4 frequency bins. The complexity of the DFT is of the order of $10^4 L_p$. With $L_p = 250$ and $L_p = 500$, this translates to 2.5×10^6 and 5×10^6 operations respectively. We now propose a two-step approach to reduce the complexity. In the first step, we divide 0.4 radians into B_1 frequency bins and the length of the DFT is taken to be $L_1 < L_p$. The resolution of the first step is thus $0.4/B_1$ radians. Let $\omega_{\text{ML},1}$ denote the estimate of ω_f in the first step of the ML approach. In the second step, the search interval is taken as

$$\pm 8 \times \frac{0.4}{B_1} \quad (48)$$

about $\omega_{\text{ML},1}$, to ensure that the maximum estimation error lies within the search interval. This is evident from column (c) of Tables III and IV for the parameters given in (49) below. The search interval in (48) is divided into B_2 frequency bins and the length of the DFT is $L_p - L_{\text{ISI}}$, as given in (46). The complexity of the two-step approach is of the order of $L_1 B_1 + L_p B_2$. In the simulations, we have taken

$$\begin{aligned} L_1 &= 100 \\ B_1 &= 800 \\ B_2 &= 200 \end{aligned} \quad (49)$$

so that the final resolution is equal to

$$16 \times \frac{0.4}{B_1 B_2} = 4 \times 10^{-5} \text{ radians} \quad (50)$$

which is identical to the single stage ML approach. With $L_p = 250$ and $L_p = 500$, this translates to 1.3×10^5 and 1.8×10^5 operations respectively, which is more than an order of magnitude reduction in complexity. This is shown in Table V. We emphasize that L_1 , B_1 and B_2 have not been optimized to minimize the complexity. In fact, we can even have more than two steps for reducing the complexity. This could be a subject for future research. In any case, let $\hat{\omega}_f$ denote the estimate of ω_f in the second step.

The received samples $r(nT'_s)$ are demodulated again using the local oscillator frequency equal to $\pi/2 + \hat{\omega}_3 + \hat{\omega}_f$. From column (d) of Table III we find that the RMS estimation error for the ML method is 1.52×10^{-4} , for $L_p = 250$. The average phase change over the preamble is $1.52 \times 10^{-4} \times 250 \times 4 = 0.152$ radians. Similarly, from column (d) of Table IV, we obtain the average phase change over the preamble as $5.3 \times 10^{-5} \times 500 \times 4 = 0.106$ radians. These results imply that the phase can be considered to be constant over the duration of the preamble, thereby facilitating the use of the correlation method for estimating the start of frame for the third time. This feature (phase being constant over a large number of symbols) also enables the use of narrowband lowpass filters in the phase tracking loop, to average out the effects of noise. The symbol amplitude and the noise variance estimates (which is required for turbo decoding) are the by-products of the correlation method. These issues are discussed next.

TABLE V
COMPARISON OF THE COMPLEXITY OF THE SINGLE-STEP AND TWO-STEP ML METHOD OF ESTIMATING ω_f . IN BOTH CASES, THE FINAL RESOLUTION IS $\omega_s = 4 \times 10^{-5}$ RADIAN.

L_p	ML single step $10^4 L_p$	ML two-step $L_1 B_1 + L_p B_2$
250	2.5×10^6	1.3×10^5
500	5×10^6	1.8×10^5

Let $x_3(nT'_{s1})$ denote the samples at the matched filter output after demodulation by $\pi/2 + \hat{\omega}_3 + \hat{\omega}_f$. Define

$$\begin{aligned} \tilde{\mu}_3(n, k) &= \tilde{x}_3(nT'_{s1}) \tilde{\beta}^*(kT) / \left| \tilde{\beta}(kT) \right|^2 \\ \tilde{y}_3(nT'_{s1}) &= \sum_{i=0}^{L_p - L_{\text{ISI}}} \tilde{\mu}_3(n + iMI, i). \end{aligned} \quad (51)$$

The correlation method for estimating the start of frame can be stated as:

$$|\tilde{y}_3(n_3 T'_{s1})|^2 = \max_n |\tilde{y}_3(n T'_{s1})|^2 \quad (52)$$

where $n_3 T'_{s1}$ is the third estimate of t_0 . Observe that

$$\begin{aligned} \tilde{x}_3(n_3 T'_{s1} + kT) &= \tilde{\beta}(kT) e^{j((\omega_f - \hat{\omega}_f)Mk + \theta_0)} + \tilde{v}_3(n_3 T'_{s1} + kT) \\ &\approx \tilde{\beta}(kT) e^{j\theta_0} + \tilde{v}_3(n_3 T'_{s1} + kT) \quad \text{for } 0 \leq k \leq L_p - 1 \end{aligned} \quad (53)$$

since the phase change over L_p symbols due to the residual frequency offset, $\omega_f - \hat{\omega}_f$, can be neglected and $\tilde{v}_3(\cdot)$ denotes the noise term which has the property [29]:

$$(1/2)E[\tilde{v}_3(nT'_{s1} + kT)\tilde{v}_3^*(nT'_{s1} + kT - mT)] = N_0 \delta_K(mT). \quad (54)$$

Assuming that $\delta = 0$, $\omega_f = \hat{\omega}_f$ and $t_0 = n_3 T'_{s1}$, and in the absence of noise we have

$$\begin{aligned} \tilde{y}_3(n_3 T'_{s1}) &= e^{j\theta_0} \sum_{i=0}^{L_p - L_{\text{ISI}}} \left| \tilde{\beta}(iT) \right|^2 / \left| \tilde{\beta}(iT) \right|^2 \\ &= e^{j\theta_0} (L_p - L_{\text{ISI}} + 1). \end{aligned} \quad (55)$$

Therefore

$$\hat{\theta}_0 = \arg[\tilde{y}_3(n_3 T'_{s1})]. \quad (56)$$

The symbol amplitude (in our case is unity) is estimated as:

$$\hat{A} = \frac{1}{L_p - L_{\text{ISI}} + 1} \Re \left\{ \tilde{y}_3(n_3 T'_{s1}) e^{-j\hat{\theta}_0} \right\}. \quad (57)$$

The noise variance is estimated as follows:

$$\begin{aligned} \hat{\sigma}^2 &= \frac{1}{2(L_p - L_{\text{ISI}} + 1)} \sum_{k=0}^{L_p - L_{\text{ISI}}} \left(\Re \left\{ \tilde{x}_3(n_3 T'_{s1} + kT) e^{-j\hat{\theta}_0} \right\} S_{k,I} - \hat{A} \right)^2 \\ &\quad + \left(\Im \left\{ \tilde{x}_3(n_3 T'_{s1} + kT + T/2) e^{-j\hat{\theta}_0} \right\} S_{k,Q} - \hat{A} \right)^2. \end{aligned} \quad (58)$$

Note that

$$\begin{aligned}\tilde{x}_3(n_3 T'_{s1} + kT + T/2) &= (\gamma_{k,I} + j S_{k,Q}) e^{j((\omega_f - \hat{\omega}_f)(Mk + M/2) + \theta_0)} + \tilde{v}_3(n_3 T'_{s1} + kT + T/2) \\ &\approx \tilde{\beta}(kT + T/2) e^{j\theta_0} + \tilde{v}_3(n_3 T'_{s1} + kT + T/2) \quad \text{for } 0 \leq k \leq L_p - 1\end{aligned}\quad (59)$$

where $\gamma_{k,I}$ denotes the ISI in the in-phase arm. The mean and variance of the amplitude and noise variance estimates are discussed in the appendix.

This completes the acquisition of the carrier frequency, symbol timing and estimation of the symbol amplitude, carrier phase and noise variance using the preamble. In the next subsection, we discuss the algorithms for decision directed tracking of the carrier phase and timing, along with data detection.

C. Decision Directed Tracking of the Timing and Carrier Phase

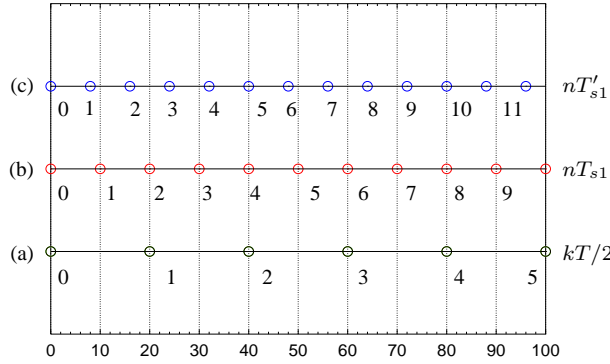


Fig. 10. (a) Offset QPSK symbols occur at times $kT/2$. (b) Samples taken at an interval of $T_{s1} = T/4$. Observe that the in-phase and quadrature symbols are obtained at times 0 and 2-mod 4 respectively. (c) Samples taken at an interval of $T'_{s1} = 0.8T_{s1}$. The receiver does not know T'_{s1} , and it assumes that its sampling period is $T_{s1} = T/4$, that is, 4 samples per symbol. However, now the 1st in-phase symbol is obtained at time 0-mod 4, the 1st quadrature symbol at time 2-mod 4, the 2nd in-phase symbol at time 1-mod 4 and so on. Therefore, the sampling instant changes mod-4. In any case, note that the symbols are obtained at times approximately equal to $kT/2$, independent of the sampling interval.

Based on (13), the sampling interval at the matched filter output is:

$$T'_{s1} = 1/F'_{s1} = T_{s1}(1 \mp 2\delta \times 10^{-6}) \triangleq T_{s1} + \epsilon'. \quad (60)$$

Since

$$nT'_{s1} = nT_{s1} + n\epsilon' \quad (61)$$

a sample is gained or lost (in other words, the sampling instant changes) at the matched filter output when

$$\begin{aligned}n\epsilon' &\geq T_{s1} \\ \Rightarrow n &\geq 10^6/(2\delta) \quad \text{samples.}\end{aligned}\quad (62)$$

The term “sampling instant” refers to the time when a symbol is recovered at the matched filter output. This is illustrated in Figure 10(c) for $\epsilon' = -0.2T_{s1}$. In a more realistic situation where $\delta = 25$ ppm, we get

$$n \geq 20000 \quad \text{samples} \equiv 20000/(MI) \quad \text{symbols} = 1250 \quad \text{symbols} \quad (63)$$

for $M = I = 4$. Thus, a sample is gained or lost (the sampling instant-mod MI changes) every 1250 symbols (recall that there are nominally MI samples per symbol at the matched filter output). Since the preamble length is only $L_p = 250$ or $L_p = 500$, there is no change in the sampling instant during the preamble. Therefore, there is no need to track the timing during the preamble. Similarly, there is no need to track the carrier phase during the preamble, since the residual frequency offset, $\omega_f - \hat{\omega}_f$ is small enough, such that the carrier phase can be considered to be nearly constant (refer to column (d) of Tables III, IV and (53), (59)). However, the data portion L_d is much larger than L_p (in our case ten times), hence both timing and carrier need to be tracked. This is the subject of this subsection.

Let

$$t_1 = t_0 + L_p T \approx n_3 T_{s1} + L_p T \approx n_3 T'_{s1} + L_p T \quad (64)$$

where t_0 is defined in (31) and $n_3 T'_{s1}$ is defined in (52). Then, the first (in-phase) data symbol is obtained at time t_1 . Let

$$\omega_r = \omega_f - \hat{\omega}_f. \quad (65)$$

The output of the sampler can be expressed as:

$$\tilde{x}_3(t_0 + kT/2) = \tilde{\beta}(kT/2)e^{j\theta(kT/2)} + \tilde{v}_3(t_0 + kT/2) \quad \text{for } 0 \leq k \leq 2(L_p + L_d) - 1 \quad (66)$$

where it is understood that the in-phase and quadrature symbols are detected when k is even and odd respectively and

$$\theta(kT/2) = \omega_r M k/2 + \theta_0 \quad \text{for } 0 \leq k \leq 2(L_p + L_d) - 1. \quad (67)$$

The data-aided phase tracking loop operates at symbol-rate ($k = 2l$) as follows [31]:

$$\begin{aligned} \tilde{z}(t_1 + lT) &= \tilde{x}_3(t_1 + lT) \left(\hat{\beta}(L_p T + lT) \right)^* \bigg/ \left| \hat{\beta}(L_p T + lT) \right|^2 \\ \tilde{z}_{\text{avg}}(t_1 + lT) &= \rho_c \tilde{z}_{\text{avg}}(t_1 + (l-1)T) + (1 - \rho_c) \tilde{z}(t_1 + lT) \\ \hat{\theta}(lT) &= \arg[\tilde{z}_{\text{avg}}(t_1 + lT)] \quad \text{for } -L_{\text{ISI}} + 1 \leq l \leq L_d - 1 \end{aligned} \quad (68)$$

where $\hat{\beta}(\cdot)$ is the estimate of $\tilde{\beta}(\cdot)$. The parameter ρ_c was taken to be 0.97 for $L_p = 250$ and 0.98 for $L_p = 500$. Note that $\hat{\theta}(lT)$ in (68) is computed in the range $[0, 2\pi)$, hence there is no phase ambiguity.

Observe that $\tilde{z}_{\text{avg}}(\cdot)$ in (68) is computed recursively. Its initial value is set to zero at the beginning of the preamble. During the preamble, it is recursively computed at symbol-rate as follows:

$$\begin{aligned} \tilde{z}(t_0 + lT) &= \tilde{x}_3(t_0 + lT) \left(\tilde{\beta}(lT) \right)^* \bigg/ \left| \tilde{\beta}(lT) \right|^2 \\ \tilde{z}_{\text{avg}}(t_0 + lT) &= \rho_c \tilde{z}_{\text{avg}}(t_0 + (l-1)T) + (1 - \rho_c) \tilde{z}(t_0 + lT) \quad \text{for } 0 \leq l \leq L_p - L_{\text{ISI}} \\ \hat{\theta}(lT) &= \arg[\tilde{z}_{\text{avg}}(lT)] \quad \text{for } l = L_p - L_{\text{ISI}}. \end{aligned} \quad (69)$$

After the preamble, $\tilde{z}_{\text{avg}}(\cdot)$ is used in (68).

Finally, the QPSK symbols at time $i = l + L_{\text{ISI}}$ are estimated as follows (note that $\tilde{\beta}(\cdot)$ in (68) is a function of $L_{\text{ISI}} - 1$ future symbols, as given in (34) and Figure 8, hence we assume that these symbols have already

been estimated):

$$\begin{aligned}\hat{S}_{i,I} &= \text{sgn} \left[\Re \left\{ \tilde{x}_3(t_1 + iT) e^{-j\hat{\theta}(lT)} \right\} \right] \\ \hat{S}_{i,Q} &= \text{sgn} \left[\Im \left\{ \tilde{x}_3(t_1 + iT + T/2) e^{-j\hat{\theta}(lT)} \right\} \right] \quad \text{for } 0 \leq i \leq L_d - 1\end{aligned}\quad (70)$$

where $\text{sgn}[\cdot]$ denotes the signum function.

Similarly the algorithm which tracks the timing, operates at symbol-rate, and is initiated during the preamble. This algorithm tracks the autocorrelation peak, $R_{pp}(0)$, which may lie in-between consecutive samples of nT'_{s1} . We denote the sampling instant for obtaining the in-phase part of a symbol as lT (see Figure 10(c)). Define for $0 \leq l \leq L_p - 1$

$$u(lT + iT'_{s1}) = \Re \left\{ \tilde{x}_3(t_0 + lT + iT'_{s1}) e^{-j\hat{\theta}_0} \right\} S_{l,I} \quad \text{for } -2 \leq i \leq 2 \quad (71)$$

where $i = 0$ denotes the “middle” sample (the correct sampling instant), $i < 0$ denotes the “early” samples and $i > 0$ denotes the “late” samples. Compute for $0 \leq l \leq L_p - 1$

$$u_{\text{avg}}(lT + iT'_{s1}) = \rho_t u_{\text{avg}}((l-1)T + iT'_{s1}) + (1 - \rho_t) u(lT + iT'_{s1}) \quad \text{for } -2 \leq i \leq 2. \quad (72)$$

The initial value of $u_{\text{avg}}(\cdot)$ is set to zero. For $L_p \leq l \leq L_p + L_d - 1$ we have

$$u(lT + iT'_{s1}) = \Re \left\{ \tilde{x}_3(t_0 + lT + iT'_{s1}) e^{-j\hat{\theta}((l-L_{IS1})T)} \right\} \hat{S}_{l,I} \quad \text{for } -2 \leq i \leq 2 \quad (73)$$

where $\hat{S}_{l,I}$ obtained from (70). Note that the averaging in (72) is done to reduce the effects of noise and ISI.



Fig. 11. The array elements are labeled $u_{\text{avg}}(lT + iT'_{s1})$ $-2 \leq i \leq 2$.

As mentioned earlier, timing is not tracked during the preamble, it is only acquired. Tracking is done during the data part as given below. We assume that the values of $u_{\text{avg}}(lT + iT'_{s1})$ are stored in an array as shown in Figure 11.

- 1) For the current sampling instant $\approx lT$, for $L_p \leq l \leq L_p + L_d - 1$, find the maximum of $u_{\text{avg}}(lT + iT'_{s1})$ for $-1 \leq i \leq 1$ (not $-2 \leq i \leq 2$), since we expect the sampling instant to change by only one sample at a time.
- 2) If $u_{\text{avg}}(lT + iT'_{s1})$ is maximum, set $c = i$, for $-1 \leq i \leq 1$
- 3) Obtain the quadrature symbol at time $lT + MIT'_{s1}/2 \approx lT + T/2$ (after $MI/2$ samples)
- 4) Do the following:
 - a) If $c = 1$, left-shift the contents of the array by one place and initialize $u_{\text{avg}}(lT + 2T'_{s1}) = 0$.
 - b) Else if $c = -1$, right-shift the contents of the array by one place and initialize $u_{\text{avg}}(lT - 2T'_{s1}) = 0$.
- 5) The next in-phase symbol is obtained at time $lT + MIT'_{s1} + cT'_{s1} \approx (k+1)T$ (after $MI + c$ samples)
- 6) Reset $c = 0$ and go back to step (1) with $l = l + 1$

Finally, the noisy symbols are obtained from (70) with the signum function removed, and fed to the BCJR algorithm [29] for turbo decoding. The details of the BCJR algorithm will not be discussed here. Having

presented the various receiver algorithms, it becomes necessary to discuss the receiver complexity. This is done in the next subsection.

D. Receiver Complexity

We begin by discussing the complexity of demodulation and matched filtering. Recall that this operation has to be done thrice. However the first two times, demodulation needs to be done only over the preamble. During the third attempt, demodulation needs to be done over the preamble and the data. The length of the matched filter is 97 samples (taken at a sampling frequency of F_{s1}), the interpolation factor $I = 4$ and the number of samples per symbol at the input of the receiver is nominally $M = 4$. Hence the number of samples per symbol at the matched filter output is nominally $MI = 16$. For obtaining each complex output sample $(97/4) \times 2 \approx 48$ real multiplications and 48 real additions are required. Therefore for obtaining all the samples corresponding to the preamble, $48 \times 3 \times L_p MI$ real multiplications and the same number of real additions are required for the three demodulation steps. During the third step, the complexity of demodulating the data is $48 \times L_d \times 5$ real multiplications and the same number of additions, since only five samples per symbol are computed (see subsection III-C). We assume that the sine and cosine operations are performed using a table lookup. Next, we look into the complexity of the differential correlation method.

For computing μ_1 in (36), one complex multiplication is involved. Therefore, for computing $\tilde{y}_1(nT_{s1})$ in (36), approximately $2L_p$ complex multiplications and L_p complex additions are involved. Note that until a burst is detected, the only operations performed by the receiver are demodulation and differential correlation. The correlation method, used to detect the start of frame for the third time requires L_p complex multiplications and the same number of complex additions. The complexity of the ML method of frequency offset estimation has been discussed in subsection III-B. The complexity of turbo decoding can be found in [29].

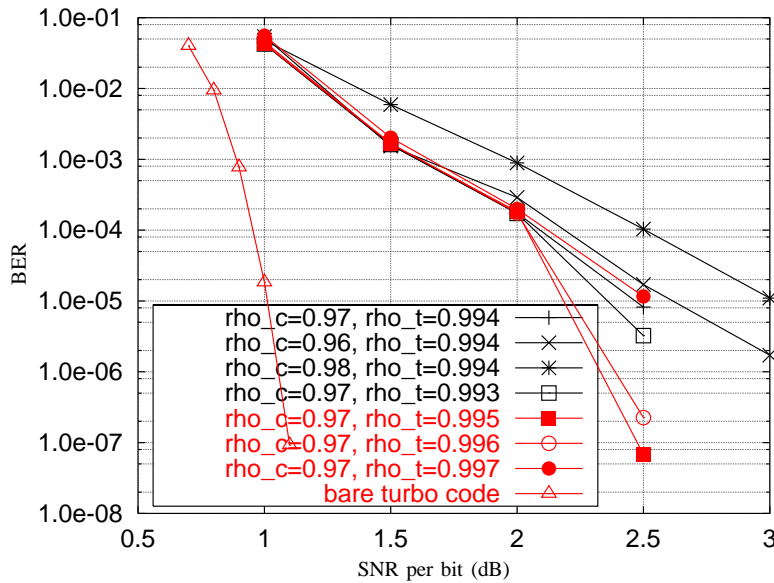


Fig. 12. BER performance for $L_p = 250$.

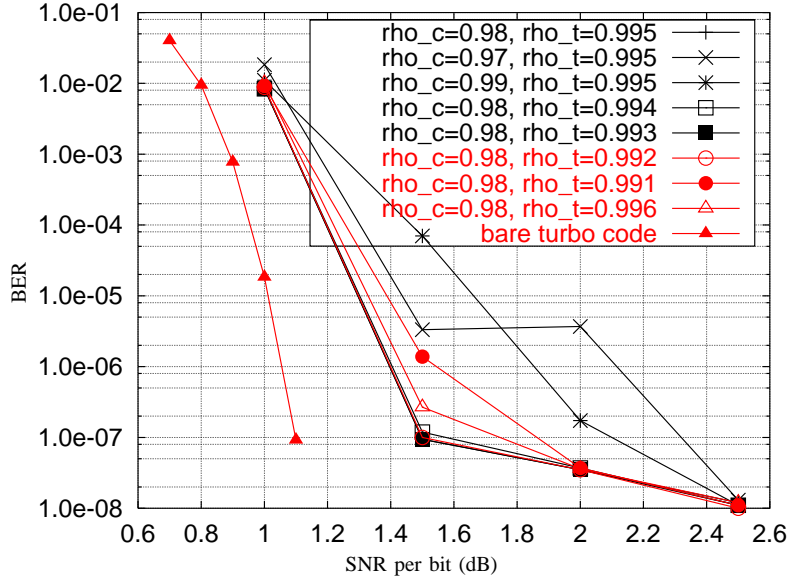


Fig. 13. BER performance for $L_p = 500$.

IV. SIMULATION RESULTS

In the simulations, $p(t)$ was taken to be the pulse having the root-raised cosine spectrum with a roll-off of 0.4 and truncated to $N + 1 = 25$ samples. The parameter $T/T_s = M = 4$ samples per symbol and interpolation factor $I = 4$. Further $L_p = 250, 500$, $L_d = 10^4$ and $L_o = 12$ QPSK symbols. Simulations were carried out over 10^5 frames (total of 10^9 data bits). The frequency offset $\omega_3 = 0.15\pi$ (refer to the sentence after (17)). We assume that α is uniformly distributed in $[0, T)$ in the BER simulations. The clock error in the transmitter and receiver is $\delta = 25$ ppm, so that the resulting offset is $2\delta = 50$ ppm. The SNR per bit is defined as [29]:

$$E_b/N_0 = 10 \log_{10} (|S_k|^2 / (2N_0)) . \quad (74)$$

Finally, the BER results are presented in Figures 12 and 13 for $L_p = 250$ and $L_p = 500$ respectively. For $L_p = 250$, $\rho_c = 0.97$ and $\rho_t = 0.995$ were found to be optimum. Similarly for $L_p = 500$, $\rho_c = 0.98$ and $\rho_t = 0.995$ were found to be optimum. The performance loss at a BER of 10^{-7} is about 1.5 dB for $L_p = 250$. However, the performance loss is only about 0.5 dB for $L_p = 500$, for the same BER. For $L_p = 500$ the BER is less than 10^{-9} for an SNR per bit of 3 dB. Hence there is no error floor.

V. CONCLUSIONS AND FUTURE WORK

In this work, we have presented discrete-time algorithms for synchronization and detection of bursty offset QPSK signals. These algorithms can be readily implemented on a DSP processor. The simulation parameters chosen in this paper may not be optimum in the sense of reducing the computational complexity without compromising the BER performance. We have also shown via simulations that the acquisition time for a burst is equal to the preamble length. Future work could be in the direction of receiver design for fading channels.

APPENDIX

A. Mean and Variance of the Amplitude and Noise Variance Estimates

Assuming that $t_0 = n_3 T_{s1}$, $\theta_0 = \hat{\theta}_0$ in (57), the mean and variance of \hat{A} is

$$\begin{aligned}
 E[\hat{A}] &= A = 1 \\
 E[(\hat{A} - 1)^2] &= \frac{1}{(L_p - L_{\text{ISI}} + 1)^2} E \left[\left(\sum_{k=0}^{L_p - L_{\text{ISI}}} \frac{1}{|\tilde{\beta}(kT)|^2} \Re \left\{ \tilde{v}_3(n_3 T_{s1} + kT) e^{-j\theta_0} \tilde{\beta}^*(kT) \right\} \right)^2 \right] \\
 &= \frac{N_0}{(L_p - L_{\text{ISI}} + 1)^2} \sum_{k=0}^{L_p - L_{\text{ISI}}} \frac{1}{|\tilde{\beta}(kT)|^2}
 \end{aligned} \tag{75}$$

where we have made use of (54) and the following relations [29]:

$$\begin{aligned}
 \tilde{v}_3(\cdot) &\triangleq v_{3,I}(\cdot) + j v_{3,Q}(\cdot) \\
 E[v_{3,I}(nT_{s1}) v_{3,Q}(mT_{s1})] &= 0 \quad \text{for all } m \text{ and } n.
 \end{aligned} \tag{76}$$

The rms error in the estimate of A is the square root of the variance computed in (75). The theoretical and simulated rms error in the amplitude estimate is shown in Table VI.

TABLE VI
THE RMS ERROR IN THE AMPLITUDE ESTIMATES AT AN SNR PER BIT OF 1 dB.

L_p	Theoretical	Simulated
250	0.04724	0.04723
500	0.033237	0.033231

Assuming that $t_0 = n_3 T_{s1}$, $\hat{\theta}_0 = \theta_0$ and $\hat{A} = A = 1$ in (58), the mean value of $\hat{\sigma}^2$ is

$$\begin{aligned}
 E[\hat{\sigma}^2] &= \frac{1}{2(L_p - L_{\text{ISI}} + 1)} \sum_{k=0}^{L_p - L_{\text{ISI}}} E \left[\left(\Re \left\{ \tilde{v}_3(n_3 T_{s1} + kT) e^{-j\theta_0} \right\} S_{k,I} \right)^2 \right. \\
 &\quad \left. + \left(\Im \left\{ \tilde{v}_3(n_3 T_{s1} + kT + T/2) e^{-j\theta_0} \right\} S_{k,Q} \right)^2 \right] \\
 &= N_0
 \end{aligned} \tag{77}$$

where

$$S_{k,I}^2 = S_{k,Q}^2 = 1. \tag{78}$$

In order to find out the variance of the estimate of N_0 define:

$$\begin{aligned}
 \psi_k &= \Re \left\{ \tilde{v}_3(n_3 T_{s1} + kT) e^{-j\theta_0} \right\} S_{k,I} \quad \text{for } 0 \leq k \leq L_p - L_{\text{ISI}} \\
 \psi_{k+L_p-L_{\text{ISI}}+1} &= \Im \left\{ \tilde{v}_3(n_3 T_{s1} + kT + T/2) e^{-j\theta_0} \right\} S_{k,Q} \quad \text{for } 0 \leq k \leq L_p - L_{\text{ISI}} \\
 L_1 &= 2(L_p - L_{\text{ISI}} + 1).
 \end{aligned} \tag{79}$$

Then

$$\hat{\sigma}^2 = \frac{1}{L_1} \sum_{k=0}^{L_1-1} \psi_k^2. \tag{80}$$

Note that ψ_k and ψ_i are uncorrelated, and being Gaussian, are also independent. Hence

$$E[\psi_k \psi_i] = \begin{cases} N_0 & \text{for } k = i \\ 0 & \text{for } k \neq i. \end{cases} \quad (81)$$

The variance of the estimate of N_0 is given by:

$$\begin{aligned} E[(\hat{\sigma}^2 - N_0)^2] &= E\left[\left(\frac{1}{L_1} \sum_{k=0}^{L_1-1} \psi_k^2 - N_0\right)^2\right] \\ &= \frac{1}{L_1^2} \sum_{k=0}^{L_1-1} \sum_{i=0}^{L_1-1} E[(\psi_k^2 - N_0)(\psi_i^2 - N_0)] \\ &= \frac{1}{L_1^2} \sum_{k=0}^{L_1-1} E[(\psi_k^2 - N_0)^2] \\ &\quad + \frac{1}{L_1^2} \sum_{k=0}^{L_1-1} \sum_{\substack{i=0 \\ i \neq k}}^{L_1-1} E[(\psi_k^2 - N_0)(\psi_i^2 - N_0)] \\ &= \frac{1}{L_1^2} \sum_{k=0}^{L_1-1} E[(\psi_k^2 - N_0)^2] \\ &= \frac{2N_0^2}{L_1}. \end{aligned} \quad (82)$$

The normalized variance of the estimate of N_0 can be defined as:

$$\frac{1}{N_0} E[(\hat{\sigma}^2 - N_0)^2] = \frac{2N_0}{L_1}. \quad (83)$$

The normalized rms error in the estimate of N_0 is the square root of the normalized variance computed in (83).

The theoretical and simulated rms error in the noise variance estimate is shown in Table VII.

TABLE VII
THE NORMALIZED RMS ERROR IN THE NOISE VARIANCE ESTIMATES AT AN SNR PER BIT OF 1 DB.

L_p	Theoretical	Simulated
250	0.05659	0.0566385
500	0.039937	0.039868

B. The BCJR Algorithm [29]

The turbo decoder is shown in Figure 14. Assuming a code-rate of 1/3 and a framesize of L , the output of the demultiplexer is:

$$\begin{aligned} r_{b1,m} &= S_{b1,m} + w_{b1,m} \\ r_{c1,m} &= S_{c1,m} + w_{c1,m} \\ r_{c2,m} &= S_{c2,m} + w_{c2,m} \\ r_{b2,m} &= r_{b2,\pi(n)} = r_{b1,n} = r_{b1,\pi^{-1}(m)} \quad \text{for } 0 \leq m, n \leq L-1 \end{aligned} \quad (84)$$

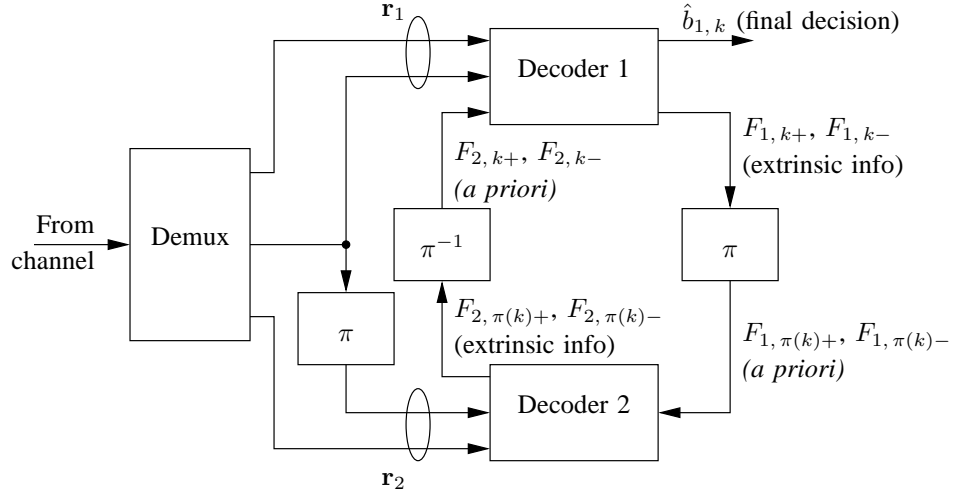


Fig. 14. The turbo decoder.

where $w_{b1,m}$, $w_{c1,m}$ and $w_{c2,m}$ are samples of zero-mean AWGN with variance σ_w^2 . Note that all quantities in (84) are real-valued. Define

$$\mathbf{r}_1 = \begin{bmatrix} r_{b1,0} & \dots & r_{b1,L-1} & r_{c1,0} & \dots & r_{c1,L-1} \end{bmatrix}^T. \quad (85)$$

In the above equation, $r_{b1,k}$ and $r_{c1,k}$ respectively denote the received samples corresponding to the uncoded symbol and the parity symbol emanating from the first encoder, at time k . Similarly

$$\mathbf{r}_2 = \begin{bmatrix} r_{b2,0} & \dots & r_{b2,L-1} & r_{c2,0} & \dots & r_{c2,L-1} \end{bmatrix}. \quad (86)$$

The BCJR algorithm for turbo decoding has the following components:

- 1) The forward recursion
- 2) The backward recursion
- 3) The computation of the extrinsic information and the final *a posteriori* probabilities.

Let \mathcal{S} denote the number of states in the encoder trellis. Let \mathcal{D}_n denote the set of states that diverge from state n . For example

$$\mathcal{D}_0 = \{0, 3\} \quad (87)$$

implies that states 0 and 3 can be reached from state 0. Similarly, let \mathcal{C}_n denote the set of states that converge to state n . Let $\alpha_{i,n}$ denote the forward SOP at time i ($0 \leq i \leq L-2$) at state n ($0 \leq n \leq \mathcal{S}-1$).

Then the forward SOP for decoder 1 can be recursively computed as follows (forward recursion):

$$\begin{aligned} \alpha'_{i+1,n} &= \sum_{m \in \mathcal{C}_n} \alpha_{i,m} \gamma_{1,\text{sys},i,m,n} \gamma_{1,\text{par},i,m,n} P(S_{b,i,m,n}) \\ \alpha_{0,n} &= 1 \quad \text{for } 0 \leq n \leq \mathcal{S}-1 \\ \alpha_{i+1,n} &= \alpha'_{i+1,n} / \left(\sum_{n=0}^{\mathcal{S}-1} \alpha'_{i+1,n} \right) \end{aligned} \quad (88)$$

where

$$P(S_{b,i,m,n}) = \begin{cases} F_{2,i+} & \text{if } S_{b,i,m,n} = +1 \\ F_{2,i-} & \text{if } S_{b,i,m,n} = -1 \end{cases} \quad (89)$$

denotes the *a priori* probability of the systematic bit corresponding to the transition from state m to state n , at decoder 1 at time i obtained from the 2^{nd} decoder at time l after deinterleaving (that is, $i = \pi^{-1}(l)$ for some $0 \leq l \leq L - 1$, $l \neq i$) and

$$\begin{aligned}\gamma_{1, \text{sys}, i, m, n} &= \exp \left[-\frac{(r_{b1, i} - S_{b, m, n})^2}{2\sigma_w^2} \right] \\ \gamma_{1, \text{par}, i, m, n} &= \exp \left[-\frac{(r_{c1, i} - S_{c, m, n})^2}{2\sigma_w^2} \right].\end{aligned}\quad (90)$$

The terms $S_{b, m, n} \in \pm 1$ and $S_{c, m, n} \in \pm 1$ denote the uncoded symbol and the parity symbol respectively that are associated with the transition from state m to state n . The normalization step in the last equation of (88) is done to prevent numerical instabilities [35].

Similarly, let $\beta_{i, n}$ denote the backward SOP at time i ($1 \leq i \leq L - 1$) at state n ($0 \leq n \leq \mathcal{S} - 1$). Then the recursion for the backward SOP (backward recursion) at decoder 1 can be written as:

$$\begin{aligned}\beta'_{i, n} &= \sum_{m \in \mathcal{D}_n} \beta_{i+1, m} \gamma_{1, \text{sys}, i, n, m} \gamma_{1, \text{par}, i, n, m} P(S_{b, i, n, m}) \\ \beta_{L, n} &= 1 \quad \text{for } 0 \leq n \leq \mathcal{S} - 1 \\ \beta_{i, n} &= \beta'_{i, n} / \left(\sum_{n=0}^{\mathcal{S}-1} \beta'_{i, n} \right).\end{aligned}\quad (91)$$

Once again, the normalization step in the last equation of (91) is done to prevent numerical instabilities.

Let $\rho^+(n)$ denote the state that is reached from state n when the input symbol is $+1$. Similarly let $\rho^-(n)$ denote the state that can be reached from state n when the input symbol is -1 . Then

$$\begin{aligned}G_{1, \text{norm}, k+} &= \sum_{n=0}^{\mathcal{S}-1} \alpha_{k, n} \gamma_{1, \text{par}, k, n, \rho^+(n)} \beta_{k+1, \rho^+(n)} \\ G_{1, \text{norm}, k-} &= \sum_{n=0}^{\mathcal{S}-1} \alpha_{k, n} \gamma_{1, \text{par}, k, n, \rho^-(n)} \beta_{k+1, \rho^-(n)}.\end{aligned}\quad (92)$$

Now

$$\begin{aligned}F_{1, k+} &= G_{1, \text{norm}, k+} / (G_{1, \text{norm}, k+} + G_{1, \text{norm}, k-}) \\ F_{1, k-} &= G_{1, \text{norm}, k-} / (G_{1, \text{norm}, k+} + G_{1, \text{norm}, k-}).\end{aligned}\quad (93)$$

Equations (88), (90), (91), (92) and (93) constitute the MAP recursions for the first decoder. The MAP recursions for the second decoder are similar.

After several iterations, the final decision regarding the k^{th} information bit obtained at the output of the 1^{st} decoder is computed as:

$$\begin{aligned}P(S_{b1, k} = +1 | \mathbf{r}_1) &= \sum_{n=0}^{\mathcal{S}-1} \alpha_{k, n} \gamma_{1, \text{par}, k, n, \rho^+(n)} \gamma_{1, \text{sys}, k, n, \rho^+(n)} F_{2, k+} \beta_{k+1, \rho^+(n)} \\ &= F_{1, k+} F_{2, k+} \exp \left(-\frac{(r_{b1, k} - 1)^2}{2\sigma_w^2} \right) \\ P(S_{b1, k} = -1 | \mathbf{r}_1) &= \sum_{n=0}^{\mathcal{S}-1} \alpha_{k, n} \gamma_{1, \text{par}, k, n, \rho^-(n)} \gamma_{1, \text{sys}, k, n, \rho^-(n)} F_{2, k-} \beta_{k+1, \rho^-(n)} \\ &= F_{1, k-} F_{2, k-} \exp \left(-\frac{(r_{b1, k} + 1)^2}{2\sigma_w^2} \right)\end{aligned}\quad (94)$$

where again $F_{2,k+}$ and $F_{2,k-}$ denote the *a priori* probabilities obtained at the output of the 2^{nd} decoder (after deinterleaving) in the previous iteration.

We have so far discussed the BCJR algorithm for a rate-1/3 encoder. In the case of a rate-1/2 encoder, the following changes need to be incorporated in the BCJR algorithm (we assume that $c_{1,i}$ is not transmitted for $i = 2k$ and $c_{2,i}$ is not transmitted for $i = 2k + 1$):

$$\begin{aligned}\gamma_{1, \text{par}, i, m, n} &= \begin{cases} \exp \left[-\frac{(r_{c1, i} - S_{c, m, n})^2}{2\sigma_w^2} \right] & \text{for } i = 2k + 1 \\ 1 & \text{for } i = 2k \end{cases} \\ \gamma_{2, \text{par}, i, m, n} &= \begin{cases} \exp \left[-\frac{(r_{c2, i} - S_{c, m, n})^2}{2\sigma_w^2} \right] & \text{for } i = 2k \\ 1 & \text{for } i = 2k + 1. \end{cases}\end{aligned}\quad (95)$$

REFERENCES

- [1] A. A. D'Amico, A. N. D'Andrea, and R. Reggiannini, "Efficient Non-Data-Aided Carrier and Clock Recovery for Satellite DVB at Very Low Signal-to-Noise Ratios," *IEEE J. on Select. Areas in Commun.*, vol. 19, no. 12, pp. 2320–2330, Dec. 2001.
- [2] F. J. Harris and M. Rice, "Multirate Digital Filters for Symbol Timing Synchronization in Software Defined Radios," *IEEE J. on Select. Areas in Commun.*, vol. 19, no. 12, pp. 2346–2357, Dec. 2001.
- [3] F. M. Gardner, "Interpolation in Digital Modems – Part I: Fundamentals," *IEEE Trans. on Commun.*, vol. 41, no. 3, pp. 501–507, Mar. 1993.
- [4] L. Erup, F. M. Gardner, and R. A. Harris, "Interpolation in Digital Modems – Part II: Implementation and Performance," *IEEE Trans. on Commun.*, vol. 41, no. 6, pp. 998–1008, June 1993.
- [5] J. D. Daley, "Improved Phase-Lock-Loop Performance at Medium to Low SNR," *Electronics Letters*, vol. 10, no. 17, pp. 365–366, Aug. 1974.
- [6] D. P. Taylor and D. C. C. Cheung, "A Decision-Directed Carrier Recovery Loop for Duobinary Encoded Offset QPSK Signals," *IEEE Trans. on Commun.*, vol. 27, no. 2, pp. 461–468, Feb. 1979.
- [7] L. E. Franks, "Carrier and Bit Synchronization in Data Communication – A Tutorial Review," *IEEE Trans. on Commun.*, vol. 28, no. 8, pp. 1107–1121, Aug. 1980.
- [8] R. W. Chang and R. Srinivasagopalan, "Carrier Recovery for Data Communication Systems with Adaptive Equalization," *IEEE Trans. on Commun.*, vol. 28, no. 8, pp. 1142–1153, Aug. 1980.
- [9] D. N. Godard, "Self-Recovering Equalization and Carrier Tracking in Two-Dimensional Data Communication Systems," *IEEE Trans. on Commun.*, vol. 28, no. 11, pp. 1867–1875, Nov. 1980.
- [10] R. L. Cupo and R. D. Gitlin, "Adaptive Carrier Recovery Systems for Digital Data Communications Receivers," *IEEE J. on Select. Areas in Commun.*, vol. 7, no. 9, pp. 1328–1339, Dec. 1989.
- [11] N. Caouras, R. Morawski, and T. Le-Ngoc, "Fast Carrier Recovery for Burst-Mode Coherent Demodulation Using Feedforward Phase and Frequency Estimation Techniques," in *Proc. of the IEEE Canadian Conference on Electrical and Computer Engineering*, Edmonton, Canada, May 1999, pp. 79–83.
- [12] S. Saito and H. Suzuki, "Fast Carrier-Tracking Coherent Detection with Dual-Mode Carrier Recovery Circuit for Digital Land Mobile Radio Transmission," *IEEE J. on Select. Areas in Commun.*, vol. 7, no. 1, pp. 130–139, Jan. 1989.
- [13] K. Kobayashi, T. Sakai, S. Kubota, M. Morikura, and S. Kato, "A New Carrier Recovery Circuit for Land Mobile Satellite Communication," *IEEE J. on Select. Areas in Commun.*, vol. 10, no. 8, pp. 1306–1314, Oct. 1992.
- [14] M. Uchishima, Y. Tozawa, T. Miyo, and S. Takenaka, "Burst DSP Demodulator for Low E_b/N_0 Operation," in *Proc. IEEE Int. Conf. on Communications*, June 1991, pp. 226–230.
- [15] K. Kobayashi, Y. Matsumoto, K. Seki, and S. Kato, "A Full Digital Modem for Offset Type Modulation Schemes," in *Proc. of the 3rd IEEE Intl. Symp. on Personal, Indoor and Mobile Radio Commun.*, Oct. 1992, pp. 596–599.
- [16] F. Lorenzelli, L. Testa, M. Visintin, E. Biglieri, and M. Pent, "Clock-Aided Carrier Recovery in Trellis-Coded PSK," *IEEE J. on Select. Areas in Commun.*, vol. 7, no. 9, pp. 1307–1317, Dec. 1989.
- [17] M. Sangriotis and I. Xezonakis, "Digital Costas Loop Like PLL for the Carrier Recovery of a QPSK Signal," *Electronics Letters*, vol. 29, no. 10, pp. 897–899, May 1993.

- [18] G. Karam, J. Kervarec, H. Sari, and P. Vandamme, "All-Digital Implementation of the Carrier Recovery Loop in Digital Radio Systems," in *Proc. IEEE Int. Conf. on Communications*, June 1991, pp. 175–179.
- [19] A. M. Benani and F. Gagnon, "Comparison of Carrier Recovery Techniques in M -QAM Digital Communication Systems," in *Proc. of the IEEE Canadian Conference on Electrical and Computer Engineering*, Mar. 2000, pp. 73–77.
- [20] K.-Y. Kim and H.-J. Choi, "Design of Carrier Recovery Algorithm for High-Order QAM with Large Frequency Acquisition Range," in *Proc. IEEE Int. Conf. on Communications*, June 2001, pp. 1016–1020.
- [21] H.-A. Hou, "Modified 128-QAM Constellation Schemes Allowing Low Complexity Non-Data Aided Carrier Recovery," in *Proc. of the 16th IEEE Intl. Symp. on Personal, Indoor and Mobile Radio Commun.*, 2005, pp. 2557–2561.
- [22] K. Feher and G. S. Takhar, "A New Symbol Timing Recovery Technique for Burst Modem Applications," *IEEE Trans. on Commun.*, vol. 26, no. 1, pp. 100–108, Jan. 1978.
- [23] B. Koblents and P. J. McLane, "Asynchronous Timing Recovery in DSP Based PSK Modems," in *Conf. Rec. 26th Asilomar Conf. on Signals, Systems and Comp.*, Oct. 1992, pp. 632–641.
- [24] K. Shi and E. Serpedin, "Fast Timing Recovery for Linearly and Non-linearly Modulated Systems," *IEEE Trans. on Veh. Technol.*, vol. 54, no. 6, pp. 2017–2023, Nov. 2005.
- [25] Y. Shirato, H. Yoshioka, and K. Watanabe, "A Novel Timing Recovery Circuit with High Tracking Ability for Burst-mode Multilevel QAM Transmission," in *IEEE Wireless Communications and Networking Conference (WCNC)*, Mar. 2005, pp. 578–583.
- [26] J. R. Barry, A. Kavčić, S. W. McLaughlin, A. Nayak, and W. Zeng, "Iterative Timing Recovery," *IEEE Sig. Proc. Mag.*, vol. 21, no. 1, pp. 89–102, Jan. 2004.
- [27] I. Bergel and A. J. Weiss, "Cramér-Rao Bound on Timing Recovery of Linearly Modulated Signals with no ISI," *IEEE Trans. on Commun.*, vol. 51, no. 4, pp. 634–640, April 2003.
- [28] W. E. Ryan, "A Turbo Code Tutorial," 1997, available online at: <http://www.ece.arizona.edu/~ryan/>.
- [29] K. Vasudevan, *Digital Communications and Signal Processing*. Universities Press (India), Hyderabad. www.universitiespress.com, 2007.
- [30] —, "DSP-Based Algorithms for Voiceband Modems," 1995, masters thesis, Indian Institute of Technology, Madras.
- [31] —, "Synchronization of Bursty Offset QPSK Signals in the Presence of Frequency Offset and Noise," in *Proc. IEEE TENCON, Hyderabad, India*, Nov. 1998.
- [32] J. G. Proakis and D. G. Manolakis, *Digital Signal Processing: Principles, Algorithms and Applications*, 2nd ed. Maxwell MacMillan, 1992.
- [33] H. Meyr, M. Moeneclaey, and S. A. Fechtel, *Digital Communication Receivers: Synchronization, Channel Estimation, and Signal Processing*, 1st ed. Wiley Interscience, 1998.
- [34] Z. Y. Choi and Y. H. Lee, "Frame Synchronization in the Presence of Frequency Offset," *IEEE Trans. on Commun.*, vol. 50, no. 7, pp. 1062–1065, July 2002.
- [35] R. Koetter, A. C. Singer, and M. Tüchler, "Turbo Equalization," *IEEE Sig. Proc. Mag.*, vol. 21, no. 1, pp. 67–80, Jan. 2004.

Publications from this Work

- K. Vasudevan, "Synchronization of Bursty Offset QPSK Signals in the Presence of Frequency Offset and Noise", *Proc. IEEE TENCON*, Nov. 2008.
- K. Vasudevan, "Iterative Detection of Turbo-coded Offset QPSK in the presence of Frequency and Clock Offsets and AWGN", *Signal, Image and Video Processing*, vol. 6, no. 4, pp. 557-567, Nov. 2012.

Masters Thesis Guided

- Deshmukh Nikhil Ashok, "Synchronization of QPSK Signals in the Presence of Frequency Offset and AWGN".
- Yugal Kishor Sahu, "Application of Turbo Codes for Geosynchronous SATCOM Channels".